




# *Toxoplasma* Shelph, a Phosphatase Located in the Parasite Endoplasmic Reticulum, Is Required for Parasite Virulence

Rania Najm,<sup>a,c</sup> Maguy Hamie,<sup>b</sup> Laurence Berry-Sterkers,<sup>c</sup> Maryse Lebrun,<sup>c</sup> Hiba El Hajj,<sup>b</sup>  Mauld H. Lamarque<sup>c</sup>

<sup>a</sup>Department of Biomedical Sciences, College of Medicine, Mohammed Bin Rashid University of Medicine and Health Sciences, Dubai, United Arab Emirates

<sup>b</sup>Department of Experimental Pathology, Immunology and Microbiology, American University of Beirut, Beirut, Lebanon

<sup>c</sup>LPHI, UMR 5235 CNRS, Université de Montpellier, Montpellier, France

**ABSTRACT** *Toxoplasma gondii* is a single-celled parasitic eukaryote that evolved to successfully propagate in any nucleated cell. As with any other eukaryote, its life cycle is regulated by signaling pathways controlled by kinases and phosphatases. *T. gondii* encodes an atypical bacterial-like phosphatase absent from mammalian genomes, named Shelph, after its first identification in the psychrophilic bacterium *Schewanella* sp. Here, we demonstrate that *Toxoplasma* Shelph is an active phosphatase localized in the parasite endoplasmic reticulum. The phenotyping of a *shelph* knockout (KO) line showed a minor impairment in invasion on human fibroblasts, while the other steps of the parasite lytic cycle were not affected. In contrast with *Plasmodium* ortholog Shelph1, this invasion deficiency was not correlated with any default in the biogenesis of secretory organelles. However, Shelph-KO parasites displayed a much-pronounced defect in virulence *in vivo*. These phenotypes could be rescued by genetic complementation, thus supporting an important function for Shelph in the context of a natural infection.

**IMPORTANCE** *Toxoplasma gondii* belongs to the *Apicomplexa* phylum, which comprises more than 5,000 species, among which is *Plasmodium falciparum*, the notorious agent of human malaria. Intriguingly, the *Apicomplexa* genomes encode at least one phosphatase closely related to the bacterial *Schewanella* phosphatase, or Shelph. To better understand the importance of these atypical bacterial enzymes in eukaryotic parasites, we undertook the functional characterization of *T. gondii* Shelph. Our results uncovered its subcellular localization and its enzymatic activity, revealed its subtle involvement during the tachyzoite invasion step of the lytic cycle, and more importantly, highlighted a critical requirement of this phosphatase for parasite propagation in mice. Overall, this study revealed an unexpected role for *T. gondii* Shelph in the maintenance of parasite virulence *in vivo*.

**KEYWORDS** *Toxoplasma gondii*, enzyme kinetics, infectious disease, parasitology, reverse genetic analysis, serine/threonine phosphatases, subcellular localization

**A** *picomplexa* parasites are pathogens of human and veterinary importance, including *Plasmodium* spp., the etiologic agent of malaria, and *Toxoplasma gondii*, which is responsible for toxoplasmosis. These obligate intracellular parasites display complex life cycles alternating between definitive and intermediate hosts, such as humans. Upon infection by *T. gondii* via the ingestion of cysts or sporulated oocysts shed in cat feces, the parasites invade enterocytes and differentiate into fast-replicating forms called tachyzoites (1). Upon invasion, they establish a surrounding vacuole within the host cell and start replicating in this niche. At the end of the multiplication process, the newly formed daughter cells egress from the host and can initiate another cycle. The iteration of this lytic cycle causes massive cellular destruction and simultaneously triggers a proinflammatory host response (2–4). It is believed that under the pressure of the immune system, the parasite converts into slow-replicating dormant stages called bradyzoites that form tissue cysts primarily in

**Editor** Silvia N. J. Moreno, University of Georgia

**Copyright** © 2022 Najm et al. This is an open-access article distributed under the terms of the [Creative Commons Attribution 4.0 International license](https://creativecommons.org/licenses/by/4.0/).

Address correspondence to Mauld H. Lamarque, [mauld.lamarque@umontpellier.fr](mailto:mauld.lamarque@umontpellier.fr).

The authors declare no conflict of interest.

**Received** 18 July 2022

**Accepted** 16 October 2022

**Published** 3 November 2022

the brain and skeletal muscles (5). These cysts persist for the lifetime of the host and can reactivate into tachyzoites in immunocompromised patients.

The lytic cycle of *T. gondii* relies on reversible phosphorylation ensured by parasite kinase homologs to mammalian enzymes, such as protein kinase G (PKG) or protein kinase A (PKA), which regulate egress (6–11), replication (11, 12), invasion (13), and the transition from tachyzoite to bradyzoite (14–16). In addition to these well-conserved kinases, *Apicomplexa* parasites possess an expanded repertoire of plant-like kinases named calcium-dependent kinases (CDPKs) (17), of which CDPK1 and -3 have been shown to be involved in invasion and egress, respectively (18–20). In contrast to the wealth of data highlighting the importance of parasite kinases, the functions of most parasite phosphatases remains unexplored. Classically, phosphatases are subdivided into three groups: the protein phosphatases (PPP), the metallo-dependent phosphatases (PPM), and the tyrosine phosphatases (PTP) (21), the former two being serine/threonine phosphatases. The PPP family is likely very ancient, as members can be found in prokaryotes and eukaryotes, and it is further subdivided into PP1, PP2A, PP2B, PP4, PP5, PP6, PP7, and PPKL enzymes. A bioinformatic search performed on the *T. gondii* genome identified 11 PPPs and 33 PPMs (22). Among the PPP family, *Apicomplexa* genomes, with the exception of *Babesia bovis*, encode bacterial-like phosphatases that are absent from the human genome but found in plants and a red alga, *Porphyra yezoensis* (22, 23). Because of their similarity with a phosphatase of the psychrophilic bacteria *Schewanella* spp., they are named Schewanella-like phosphatases, or Shelph (Slp). In *Arabidopsis thaliana*, AtSlp1 and -2 display chloroplast and mitochondrial localization, respectively, with AtShl2 shown to regulate seed germination (24, 25). The *Plasmodium* spp. genome encodes two Slps, annotated Slp1 and Slp2, that display tyrosine phosphatase activity despite harboring most of the conserved residues found in the PPP subgroup (26, 27). In *Plasmodium berghei*, a rodent model of *Plasmodium* spp., PbSlp1 preferentially localizes to the endoplasmic reticulum (ER) and is associated with membrane fractions (27). Although dispensable for asexual development and gametocytogenesis in red blood cells, PbSlp1 knockout (KO) parasites were impaired in ookinete conversion *in vitro* and were unable to form oocysts in the mosquito midgut epithelium (27). Ultrastructural analysis of PbSlp1-KO ookinetes revealed a major defect in apical microneme formation, suggesting a potential role for PbSlp1 in microneme maturation and/or trafficking of micronemal proteins. In *Plasmodium falciparum*, PFSlp2 is a late-expressed protein during the erythrocytic cycle, is apically localized in merozoites, and is likely secreted in the host at the time of invasion (26, 28). However, PFSlp2-KO parasites did not exhibit any defect during asexual development, suggesting that its function may be either compensated by another phosphatase or relevant in other stages of the *P. falciparum* life cycle.

Among the 44 serine/threonine phosphatases identified *in silico* in the *T. gondii* genome, only one Slp protein was identified (22). A recent functional study performed on 17 phosphatases of *T. gondii* reported Slp localization in the cytoplasm and dense granules of the parasite (29). In addition, deletion of the *slp* gene did not impact the parasite lytic cycle in human fibroblasts or its virulence in mice.

In this study, we investigated the localization, enzymatic activity, and function of TgSlp in tachyzoites. We found that TgSlp is an active phosphatase dispensable to complete the lytic cycle *in vitro*. However, in contrast to the published data, our results support an ER localization for TgSlp and indicate that the virulence of Slp-KO parasites is strongly attenuated in mice. Importantly, this phenotype can be rescued by genetic complementation. Altogether, our results suggest that the phosphatase fulfills an important function for parasite survival *in vivo*.

## RESULTS

**TGME49\_254770 is a putative Schewanella-like phosphatase.** *T. gondii* genome analysis revealed the presence of one Schewanella-like phosphatase ortholog (22), TGME49\_254770, that we renamed TgSlp throughout the study. Protein alignment with *P. falciparum* Slp1 and Slp2 indicated that TgSlp shares 32% identity with PFSlp1, versus 28% with PFSlp2 (see Fig. S1A and B in the supplemental material). As previously described for PFSlp,

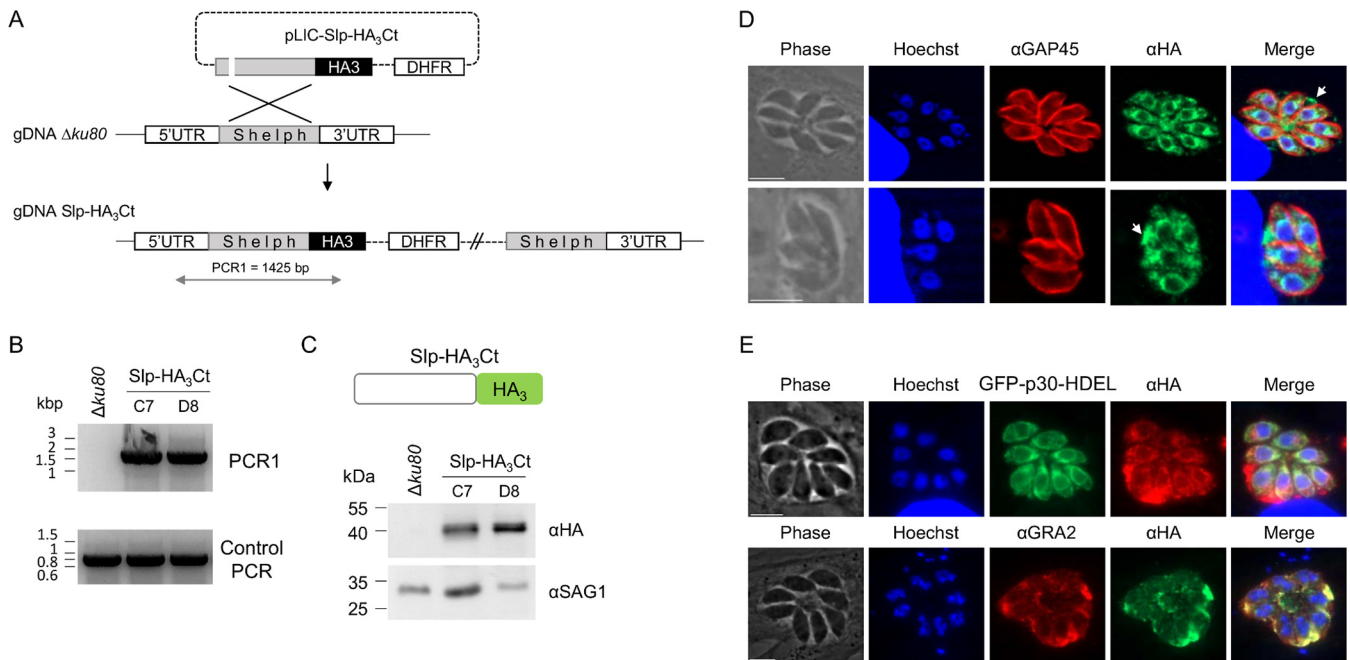


**FIG 1** Snp-HA<sub>3</sub>Ct behaves as a dense granule protein. (A) Scheme depicting the single-crossover integration of pLIC-Snp-HA<sub>3</sub>Ct at the endogenous *slp* locus. PCR1 corresponds to the integrative PCR shown in panel B. (Size of the amplicon is in base pairs.) (B) Integrative PCR for pLIC-Snp-HA<sub>3</sub>Ct genomic integration (PCR1) showing the expected 1,425-bp amplification for clones C7 and D8. The control PCR corresponds to the amplification of *ron10*. (C, top) The scheme represents Snp-HA<sub>3</sub>Ct protein with the C-terminal location of the HA<sub>3</sub> tag. (Bottom) Immunoblot of Snp-HA<sub>3</sub>Ct lines versus the parental  $\Delta ku80$  using anti-HA antibodies. SAG1, loading control. (D) IFA of Snp-HA<sub>3</sub>Ct parasites using anti-HA antibodies showing the localization of Snp-HA<sub>3</sub> protein in close proximity to the nucleus but also secreted in the PV (white arrows). GAP45, inner membrane complex marker. Nuclei were stained with Hoechst. Scale bar, 5  $\mu$ m. (E) IFA of Snp-HA<sub>3</sub>Ct parasites using anti-HA and either GFP-p30-HDEL as an ER marker or anti-GRA2 antibodies, showing a large colocalization of the proteins in the ER and the PV lumen, respectively. Nuclei were stained with Hoechst. Scale bar, 5  $\mu$ m.

*TgSnp* displays a conserved central metallo-phosphatase domain (amino acids 95 to 321) exhibiting signature motifs characteristic of the PPP family (GDXHG, GDXVDRG, and GNH[E/D]), as well as specific residues involved in metal ion coordination (Fig. S1B), suggesting that the protein is likely an active phosphatase. No signal peptide was predicted in the *TgSnp* coding sequence, but a putative transmembrane domain was sometimes predicted between amino acids 57 and 77, depending on the software used.

***TgSnp* is primarily located in the endoplasmic reticulum.** We first investigated the subcellular localization of Snp by using a ligation-independent cloning (LIC) system to add a C-terminal triple hemagglutinin tag (HA<sub>3</sub>) at the endogenous locus by single crossover in the  $\Delta ku80$  background (Fig. 1A). Diagnostic PCRs performed on two clones (C7 and D8) confirmed the correct integration of the plasmid (Fig. 1B), and the resulting fusion protein, named Snp-HA<sub>3</sub>Ct for C-terminal tagging, was detected by Western blotting as a single band of the expected molecular mass (51 kDa) (Fig. 1C). In an immunofluorescence assay (IFA), the majority of the parasites exhibited a perinuclear labeling that partially colocalized with the ER reporter GFP-p30-HDEL (Fig. 1D and E). In addition, a strong fluorescent signal was also detected in the parasitophorous vacuole (PV), which colocalized with the dense granule protein GRA2 (Fig. 1D and E), supporting *TgSnp* as a dense granule protein, as previously reported (29). However, we noticed a C-terminal GDEL motif in the protein sequence at positions 417 to 420 (Fig. S1B), reminiscent of the canonical ER retention signal H/KDEL for soluble protein retrieval to the ER (30, 31). We hypothesized that the HA<sub>3</sub> C-terminal tagging of the protein perturbed the retrieval of Snp to the ER, which as a consequence may have favored its secretion in the PV. To investigate this possibility, we used CRISPR-Cas9 technology to introduce an HA<sub>3</sub> tag 9 amino acids before the GDEL motif (Fig. 2A). The strain thereby obtained, named Snp-HA<sub>3</sub>, was verified by PCR and sequencing (Fig. 2B; Fig. S2), and the fusion protein was correctly expressed (Fig. 2C). In the IFA, the protein appeared again, staining in proximity with the nucleus that largely colocalized with the ER reporter GFP-p30-HDEL (Fig. 2D), further supporting an ER localization. Importantly, Snp-HA<sub>3</sub> was no longer

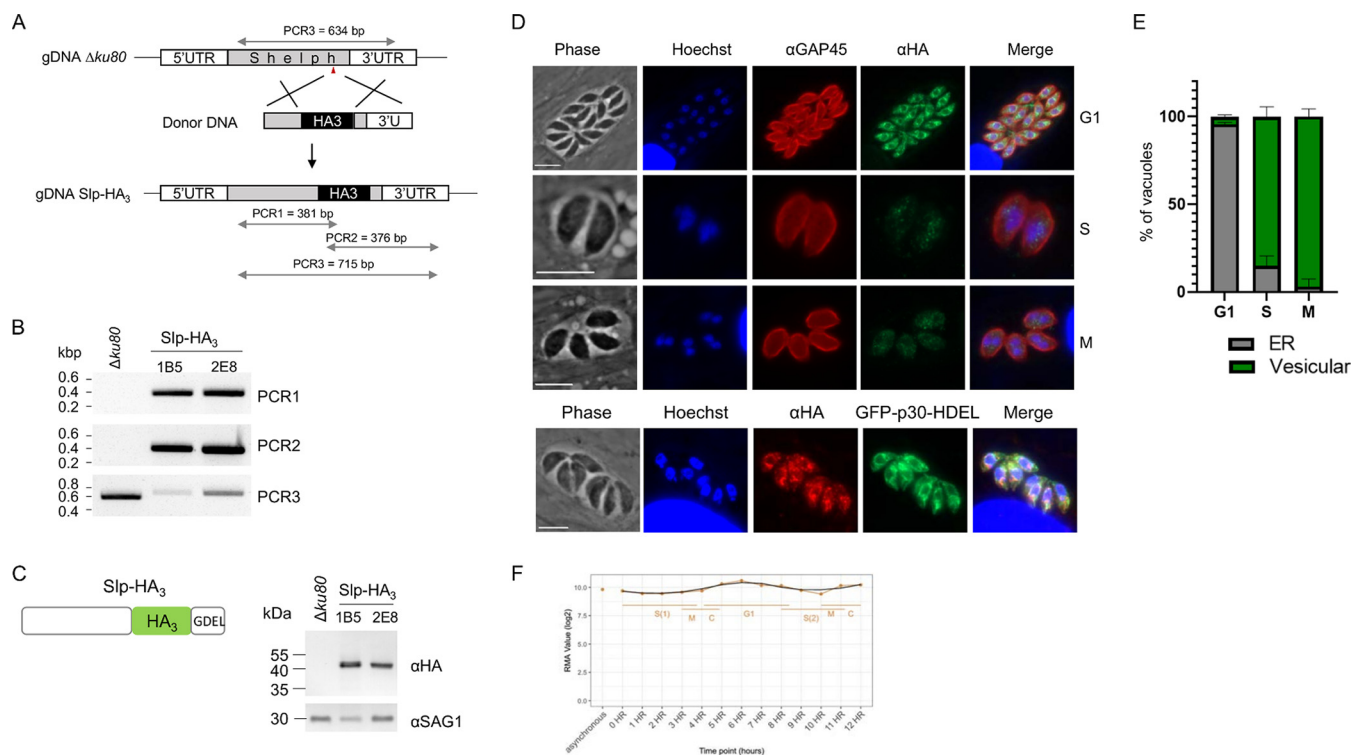


**FIG 2** Slp-HA<sub>3</sub> is an ER-resident protein. (A) Scheme showing the 2 homology regions used to insert an HA<sub>3</sub> tag 9 residues before GDEL using CRISPR-Cas9. The red arrow corresponds to the guide RNA sequence. The diagnostic PCRs used in panel B are shown below the edited genomic DNA, and the sizes of the expected amplicons are indicated in base pairs. (B) Diagnostic PCRs confirming the successful modification of the genome, performed on clones 1B5 and 2E8, as depicted in panel A. (C, left) The scheme represents Slp-HA<sub>3</sub> protein with the location of the HA<sub>3</sub> tag 9 amino acids before the C-terminal GDEL motif. (Right) Immunoblot of  $\Delta ku80$  or Slp-HA<sub>3</sub> parasites using anti-HA antibodies. SAG1, loading control. (D) IFA of Slp-HA<sub>3</sub> parasites using anti-HA and anti-GAP45 antibodies or anti-HA alone on parasites expressing the ER marker GFP-p30-HDEL. Hoechst staining and phase were used to monitor the phase of the cell cycle (G<sub>1</sub>, S, or M). Scale bar, 5  $\mu$ m. (E) Quantification of the distribution of Slp-HA<sub>3</sub> localization along the parasite cell cycle. The graph represents means of 2 quantifications  $\pm$  standard deviation. Number of vacuoles observed in G<sub>1</sub>, S, and M ( $n = 323, 78,$  and  $36,$  respectively). (F) *T. gondii* RH cell cycle microarray expression profile of *Tgslp* (45). Robust multi-array average (RMA) normalized values are shown (base log<sub>2</sub>).

detected in the PV, thereby indicating that a free C terminus is important for the proper targeting of the protein to the ER. In addition, Slp-HA<sub>3</sub> expression oscillated along the cell cycle, with parasites in G<sub>1</sub> phase exhibiting the strongest signal while those in S and M phases showed a very weak vesicular staining in the parasite cytoplasm (Fig. 2D and E). This timing of expression was in agreement with the available transcriptomic data on *Tgslp* (32) (Fig. 2F). Altogether, our results indicated that *TgSlp* is mainly localized in the ER of the parasite, which is also concordant with the recent spatial assignment of Slp by hyperLOPIT (33).

**Slp is a bona fide phosphatase.** To verify the predicted enzymatic activity of Slp phosphatase, we expressed a recombinant Slp protein in *Escherichia coli*, fused at its N terminus to a glutathione S-transferase (GST) tag (rSlp). Following affinity purification on glutathione-agarose beads of GST alone (rGST) or rSlp proteins (Fig. 3A and B), the phosphatase activities of the proteins were tested against the artificial substrate *para*-nitrophenylphosphate (pNPP) (Fig. 3C). In contrast to rGST, rSlp exhibited phosphatase activity toward pNPP with a calculated  $V_{max}$  of  $\sim 1,228 \pm 37.6$  nmol pNP/min/mg of protein (mean  $\pm$  standard error of the mean [SEM]). This result was in agreement with the range of activities reported in other organisms (26, 34).

**Slp is dispensable *in vitro* in human fibroblast cultures.** To further investigate the function of Slp, we engineered a knockout line in the Slp-HA<sub>3</sub>Ct background, using CRISPR-Cas9. Donor DNA consisted in the PCR amplification of the selectable *HXGPR*T cassette, flanked on both sides by 30-bp homology regions corresponding to *slp* 5' and 3' untranslated regions (UTRs), respectively (Fig. S3A). Edited parasites were screened by IFA for the loss of the HA signal (Fig. 4A), and the obtention of a Slp-KO line was confirmed by diagnostic PCRs and immunoblotting (Fig. S3B; Fig. 4B). In plaque assays, the Slp-KO lytic cycle was undistinguishable from that of control parasites (Fig. 4C), in agreement with a previous whole-genome screen by

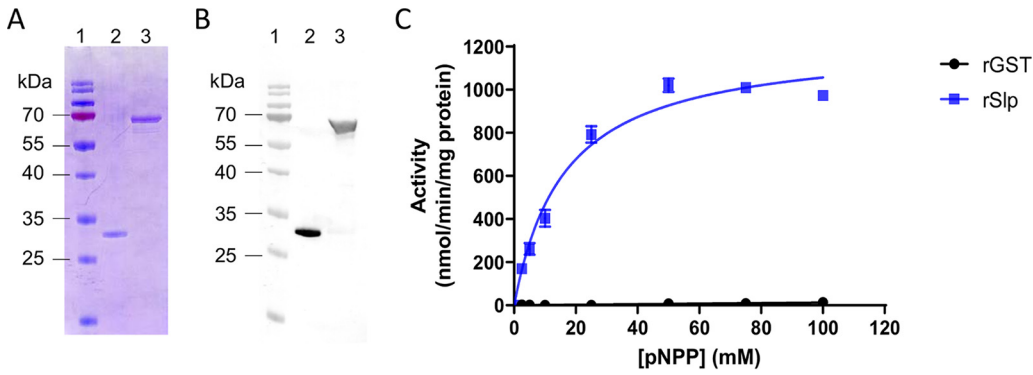


**FIG 3** Recombinant rSlp is an active phosphatase. (A) SDS-PAGE of rGST (lane 2) or rSlp (lane 3) stained with Coomassie blue. Lane 1, page ruler prestained protein ladder. (B) Immunoblot of the same proteins as in panel A revealed with anti-GST antibodies. (C) Fitted curve of the phosphatase activity of rGST or rSlp against increasing concentrations of pNPP ( $n = 4$  independent experiments, with means  $\pm$  SEM shown).

CRISPR-Cas9 of *T. gondii* tachyzoites during *in vitro* growth in fibroblasts (35). As plaque assays recapitulate several steps of the *T. gondii* lytic cycle in a single assay, slight defects may be overlooked, which prompted us to assess individually each step of the lytic cycle. The overall multiplication rate of Slp-KO was slightly faster than that of the parental line, with a consistently higher number of vacuoles containing 16 parasites (Fig. 4D). Slp-KO egress and gliding motility were undistinguishable from those observed in the parental line (Fig. 4E and F), while we noticed a moderate but reproducible decrease of the invasion capacities of the parasites by 20% (Fig. 4G). To ascertain whether the invasion defect was directly correlated with the loss of Slp, we complemented the Slp-KO line with the PSBLE35 cosmid (36), encompassing the *slp* locus (Compl line). PCR and reverse transcription-PCR (RT-PCR) confirmed the restoration of the endogenous *slp* locus and of *slp* transcript expression, respectively (Fig. S4A to C). Importantly, adding back the *slp* gene restored the full invasiveness of the parasite (Fig. 4G), thereby confirming that Slp phosphatase plays a role in invasion.

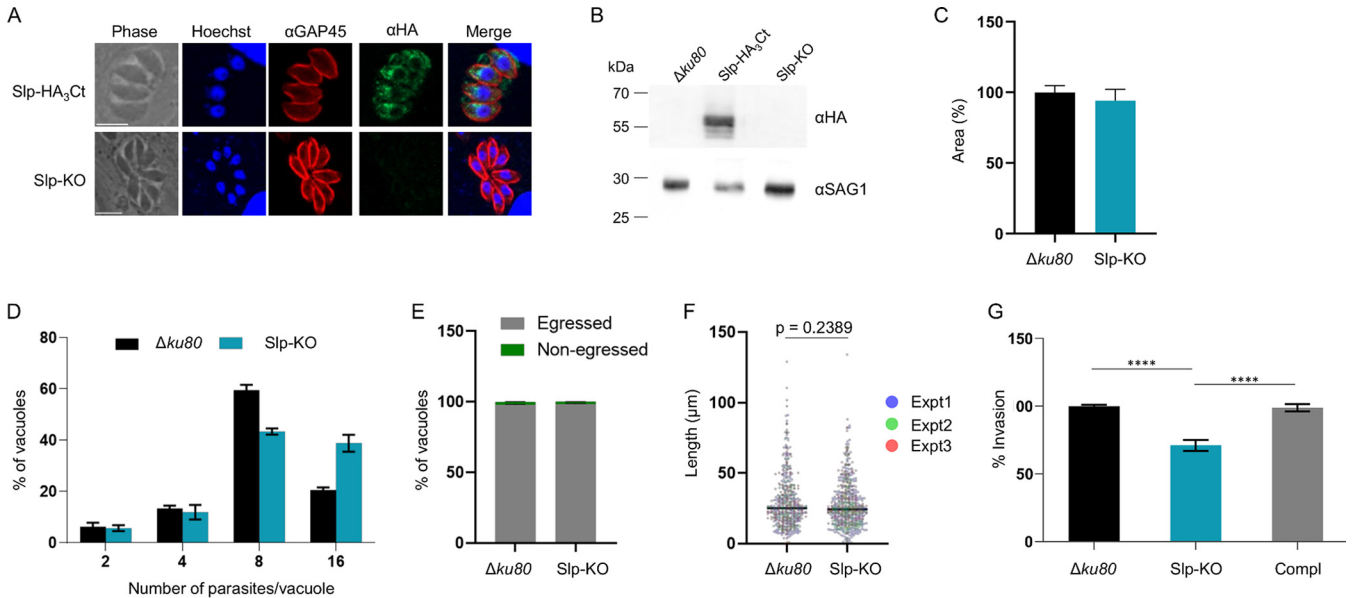


**FIG 4** Slp-KO parasites exhibit a minor defect in invasion *in vitro*. (A) IFA of Slp-HA<sub>3</sub>Ct or Slp-KO parasites using anti-HA and anti-GAP45 antibodies. Nuclei were stained with Hoechst. Scale bar, 5  $\mu$ m. (B) Immunoblot of  $\Delta ku80$ , Slp-HA<sub>3</sub>Ct, or Slp-KO parasites using anti-HA antibodies. SAG1, loading control. (C) Plaque assays performed on  $\Delta ku80$  or Slp-KO parasites. The plaque areas are expressed as percentages of the control cell line ( $n = 3$  independent experiments; means  $\pm$  SEM). (D) Replication assays performed on  $\Delta ku80$  or Slp-KO parasites ( $n = 4$  independent experiments; means  $\pm$  SEM). (E) Egress assay performed on  $\Delta ku80$  or Slp-KO parasites. Data are expressed as the percentage of vacuoles that egressed or not. The graph shows one representative experiment of two and represents the means of the experimental triplicates  $\pm$  SEM. (F) Motility assay performed on  $\Delta ku80$  or Slp-KO parasites. The graph shows the distribution of the trail lengths in 3 independent experiments. The bar represents the median, and the  $P$  value of a Mann-Whitney test is shown. (G) Invasion assay performed on  $\Delta ku80$ , Slp-KO, or Compl lines ( $n = 5$  independent experiments; mean  $\pm$  SEM). \*\*\*\*,  $P \leq 0.0001$ , Mann-Whitney test.

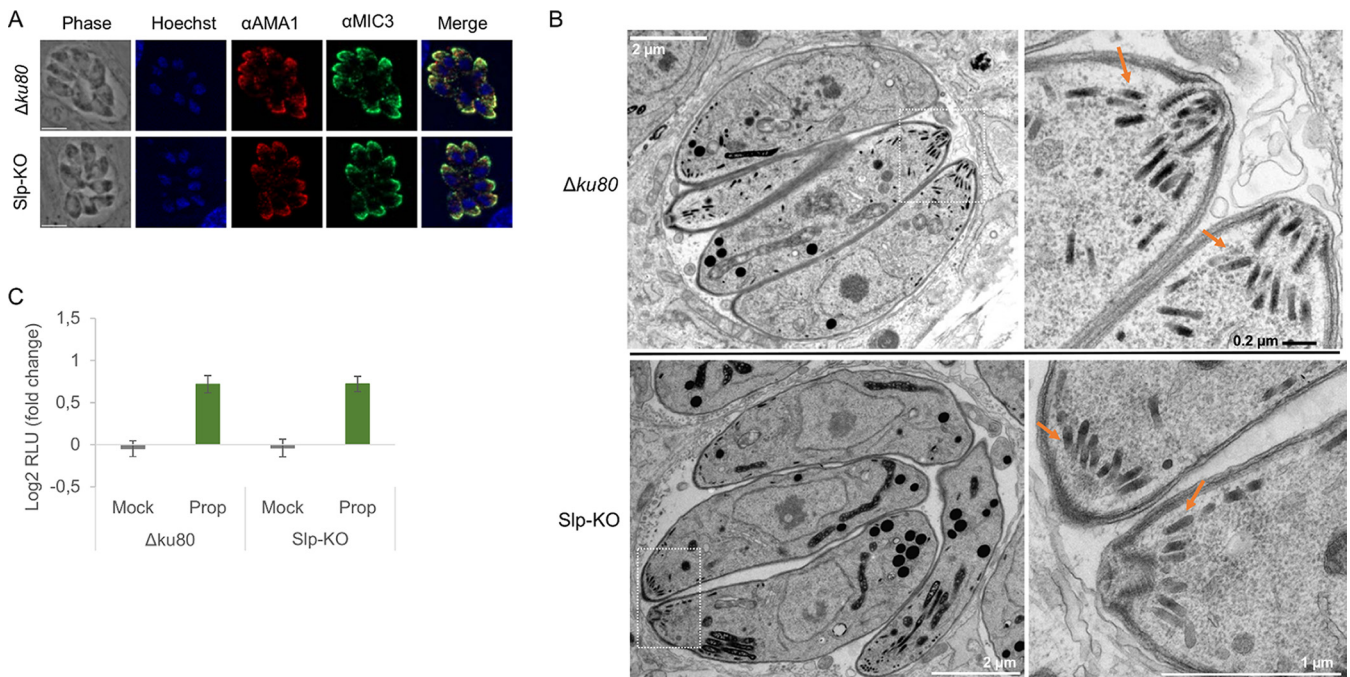


**FIG 5** Slp-KO parasites are not impaired in microneme biogenesis. (A) IFA of the micronemes in  $\Delta ku80$  or Slp-KO parasites using anti-AMA1 and anti-MIC3 antibodies. Nuclei were stained with Hoechst. Scale bar, 5  $\mu\text{m}$ . (B) Left: TEM of  $\Delta ku80$  (top) or Slp-KO intracellular tachyzoites (bottom) showing the region zoomed in as a dotted rectangle. Scale bar is indicated in each image. Right: Zoom of the apex of the tachyzoites. The orange arrows point to the micronemes. Scale bar, 1  $\mu\text{m}$  or 0.2  $\mu\text{m}$ . These are representative images of  $n = 50$  for  $\Delta ku80$  and  $n = 80$  for Slp-KO. (C) Microneme secretion assay performed on  $\Delta ku80$  or Slp-KO parasites expressing a MIC2-Gluc reporter, thereby enabling measurement of the RLU released in the medium upon microneme secretion. Data are expressed as the  $\log_2$  fold change of the RLU measured between untreated versus treated parasites with mock treatment or propranolol (prop) ( $n = 3$  independent experiments; means  $\pm$  SEM).

**Slp is not involved in microneme biogenesis.** In *P. berghei*, *PbSlp1*-KO displayed a defect in zygote-to-ookinete conversion in the mosquito midgut, with a 60% reduction in ookinete formation (27). In addition, the ookinetes that could differentiate had either no apical micronemes or a reduced number of micronemes not apically located, suggesting that *PbSlp1* may play a role in microneme biogenesis at the ookinete stage. The similar localization of *TgSlp* at the ER and the small defect of Slp-KO parasites in invasion prompted us to investigate carefully the formation of micronemes and their secretion in Slp-KO parasites. As two distinct micronemal protein subsets have been described in *T. gondii*, based on their dependence on functional Rab5A and Rab5C for their correct microneme localization (37), we first immunolocalized AMA1 and MIC3 as representative proteins of these two subsets. Both microneme subsets decorated the apex of *T. gondii* tachyzoites, regardless of the presence or absence of Slp (Fig. 5A), and no obvious defect in the number of micronemes or in their apical localization was observed by transmission electron microscopy (TEM) (Fig. 5B). To analyze the ability of the mutant to secrete the content of micronemes, we opted for a quantitative assay using a MIC2-Gaussia luciferase (MIC2-GLuc) reporter (6). Hence, we expressed MIC2-GLuc at the *uprt* locus of  $\Delta ku80$  or Slp-KO parasites (Fig. S5A). The reporter-expressing strains were verified by diagnostic PCRs (Fig. S5B). We used propranolol, an inhibitor of phosphatidic acid phosphatase, as an inducer of microneme secretion, to increase the concentration of phosphatidic acid, thereby promoting the anchoring of micronemes to the plasma membrane in an acylated pleckstrin homology domain-dependent manner (38). There was no difference in the secretion of micronemes between the control and the Slp-KO lines, further confirming that the absence of Slp does not lead to microneme defects in *T. gondii* (Fig. 5C). Similarly, we did not find evidence of any obvious deficiency regarding the rhoptries or dense granules by IFA or TEM (Fig. S6A to C).

**Slp-KO parasites are impaired in virulence *in vivo*.** Many genes encoded in the *T. gondii* genome are not essential for *in vitro* growth but yet are important for parasite survival *in vivo* (39–41). This is especially true for proteins interfering with the host immune system, such as ROPs and GRAs (42), or that are involved in specific metabolic pathways (43, 44). To

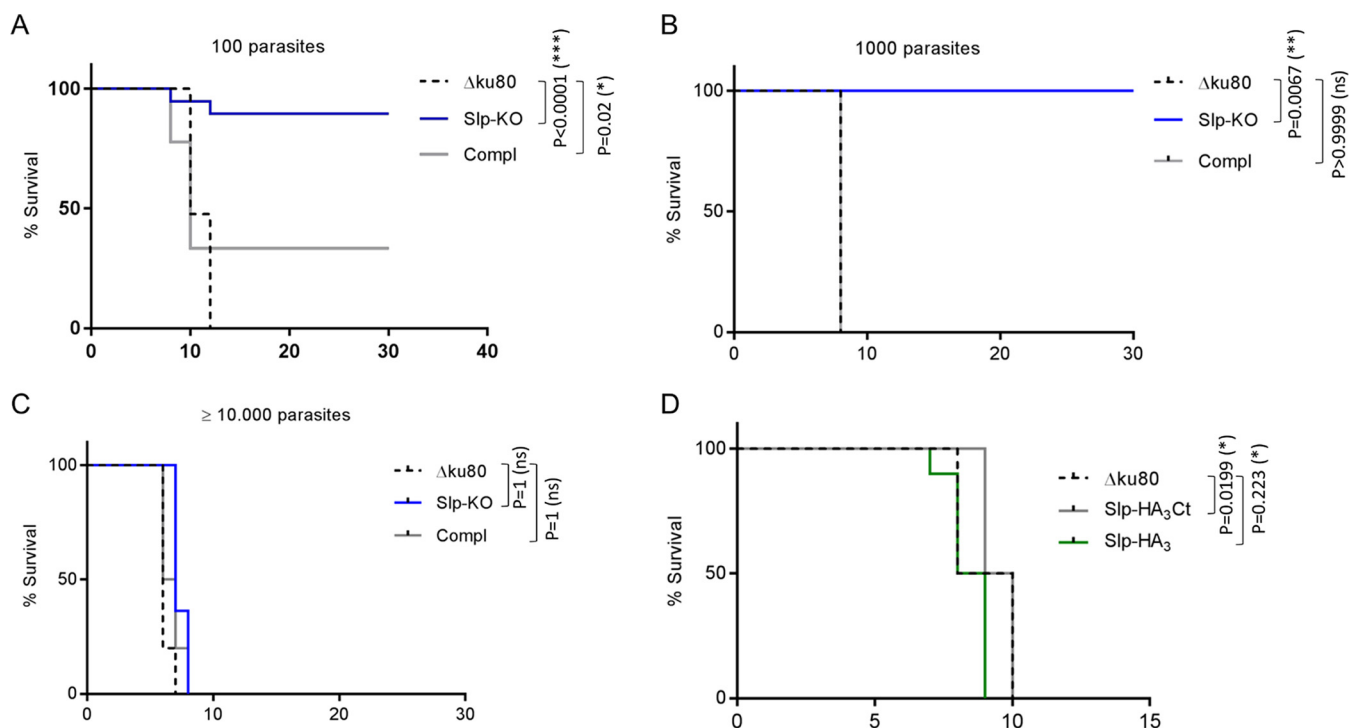


**FIG 6** SIp-KO parasites are strongly attenuated *in vivo*. (A to C) Survival of BALB/c mice infected with 100 (A), 1,000 (B), or 10,000 (C) tachyzoites of  $\Delta ku80$ , SIp-KO, or Compl parasite lines, respectively. The graphs represent the additive results of 4 (A) or 2 (B and C) independent experiments. Experimental groups: (A) 21  $\Delta ku80$  mice, 19 SIp-KO mice, 9 Compl mice; (B) 10  $\Delta ku80$  mice, 10 SIp-KO mice, and 10 Compl mice; (C) 12  $\Delta ku80$  mice, 12 SIp-KO mice, 10 Compl mice. (D) Survival of BALB/c mice infected with 100 tachyzoites of  $\Delta ku80$ , SIp-HA<sub>3</sub>Ct, or SIp-HA<sub>3</sub> parasite lines. The graph represents the additive results of 2 independent experiments ( $\Delta ku80$ , 10 mice; SIp-HA<sub>3</sub>Ct, 10 mice; SIp-HA<sub>3</sub>, 10 mice).

better define the SIp requirement during a natural infection, 100 or 1,000 tachyzoites of  $\Delta ku80$  or SIp-KO parasites were inoculated intraperitoneally into immunocompetent BALB/c mice, and their survival was monitored daily (Fig. 6A and B). While 100% of the mice succumbed to an infection with  $\Delta ku80$  within 8 to 12 days, most mice survived an infection with SIp-KO parasites. The seroconversion of the infected mice was systematically verified by Western blotting, and the seronegative mice were excluded from the analysis (Fig. S7). Importantly, the virulence was largely restored in the Compl strain. At higher parasite doses, the mice were equally susceptible to the infection (Fig. 6C). These results highlight a role for TgSIp in the maintenance of *T. gondii* virulence.

**The role of SIp in *T. gondii* virulence is independent of its localization in the PV.**

We previously demonstrated that TgSIp is an ER-resident protein and that its secretion in the PV likely represents mistargeting due to its C-terminal tagging. To assess *T. gondii* virulence when SIp is located both at the ER and in dense granules or restricted to the ER only, we infected mice with both SIp-tagged lines (SIp-HA<sub>3</sub>Ct and SIp-HA<sub>3</sub>). Both lines showed similar virulence, further supporting that the function of SIp is not linked to its association with dense granules and release in the PV (Fig. 6D).

**DISCUSSION**

Here, we have characterized a phosphatase of *T. gondii* showing similarity to bacterial phosphatase. Our data demonstrate that SIp is an active phosphatase primarily located in the ER of the parasite. Although not essential for parasite propagation in human fibroblasts *in vitro*, the SIp-KO line is slightly affected in its invasive capacity. More importantly, our data uncovered an important function for this bacterial-like phosphatase *in vivo* that may be of relevance in the context of a natural infection.

We started our characterization of SIp phosphatase by investigating its subcellular localization. The introduction of a C-terminal epitope (SIp-HA<sub>3</sub>Ct) allowed the localization of the protein at the nucleus periphery as well as in the PV lumen, where it colocalized with

the dense granule protein GRA2. These observations were concordant with those of a previous study that similarly reported partial colocalization of *TgSslp* with GRA12 in the PV of intracellular parasites (29). However, it did not fit well with the ER localization of the protein by HyperLOPIT (33). To address this discrepancy, we introduced a tag before the *TgSslp* putative ER retention signal (Sslp-HA<sub>3</sub>). In this parasite line, *TgSslp* was exclusively detected in the ER, and importantly, its expression pattern oscillated along the cell cycle, concordant with the transcriptomic data (32). Therefore, our results demonstrated that a free C terminus is important for the proper localization and timing of expression of the protein. The C-terminal GDEL sequence of *TgSslp* closely resembles the canonical KDEL motif for soluble ER protein retrieval in mammalian cells (45). Since its discovery, many variants of this motif have now been described, especially in the first position (46). Mutagenesis studies will help verify the importance of this motif for *TgSslp* subcellular localization.

In our hands, Sslp-KO parasites exhibited a minor impairment during invasion of human foreskin fibroblasts (HFFs) *in vitro*, which was reverted by complementation. The similar localization of *T. gondii* Sslp at the ER, with regard to *PbSslp1* for which a role in micronemes biogenesis had been suggested, prompted us to investigate carefully the formation of micronemes (and other secretory organelles) and microneme secretion in Sslp-KO parasites. The assembly of micronemes and rhoptries takes place *de novo* in the emerging daughter cells and relies on an unconventional trafficking process based on exocytic and endocytic machineries, during which protein synthesis and transport are intimately linked to organelle biogenesis (47–50). The biosynthesis of MIC proteins begins in the classical early secretory pathway, where they are targeted to the ER before being routed to the Golgi apparatus. From there, they are sorted into endosomal-like compartments, relying on the recognition of tyrosine-based motifs in their cytoplasmic tails (51), before eventually reaching immature promicronemes and then micronemes. Given its ER localization, Sslp may well play a role in vesicular trafficking for secretory organelle assembly. However, we did not observe any ultrastructural defect in the biogenesis, positioning, nor secretion capacity of the micronemes in Sslp-KO parasites. As *Plasmodium* merozoites and *Toxoplasma* tachyzoites both harbor many fewer micronemes than other parasite stages (ookinetes for *Plasmodium*, sporozoites and bradyzoites for *Toxoplasma*) (52), we did not exclude a role for Sslp in microneme biogenesis and trafficking in bradyzoites or feline merozoites, during which *sslp* is transcribed at a higher rate than in tachyzoites (53–55).

In contrast to the mild effect on the invasive capacity of the parasite *in vitro*, the loss of Sslp led to a 3-log reduction of *T. gondii* virulence in mice. This result diverged from that reported by Liang et al., in which the knockout of *sslp* did not affect the virulence of type I or type II parasites *in vivo* (29). The reasons for the discrepancies between the two studies are still unclear. Yet, the fact that our phenotype can be complemented by restoring the *sslp* wild-type locus clearly suggests that the observed defects are linked to the loss of the *sslp* gene itself. Many parasitic effectors secreted from dense granules and rhoptries hijack the host cell response to infection. Concordantly, the genetic disruption of these effectors usually compromises the strain virulence *in vivo*, while parasite growth remains unaffected *in vitro* (42). Here, we showed that when Sslp was restricted to an ER localization and no longer present in the dense granules and secreted in the PV, the parasite maintained its virulence *in vivo*. This suggested that Sslp function is not linked to its secretion from dense granules and therefore should not be considered a *bona fide* secreted effector of *T. gondii*.

Based on its cellular localization in the parasite ER, we hypothesized that Sslp might be required for the parasite to cope with ER stress. In mammalian cells, ER stress triggers the unfolded protein response (UPR), a mechanism that enables cells to restore ER homeostasis and thus ensures cell survival. In mammals, three ER transmembrane proteins act as molecular sensors of the accumulation of misfolded proteins, namely, PERK, ATF6, and IRE1 (56). *T. gondii* parasites lack ATF6 and IRE1 but encode a UPR sensor related to PERK (TgIF2K-A) that is localized to the ER (57–59). In mammals, PERK represses global protein synthesis by phosphorylating the eukaryotic translation initiation factor eIF2 $\alpha$  on residue serine 51 (59, 60). PERK optimal activity is regulated by *trans*-autophosphorylation (61, 62) and by the activity of an ER-located phosphatase called tyrosine phosphatase 1B (PTP-1B) (63–65). PTP-1B plays a

pleiotropic role not only in the regulation of metabolic homeostasis, but also in ER stress, as its deficiency leads to an increase in PERK-eIF2 $\alpha$  signaling (66, 67). Interestingly, *T. gondii* parasites that are unable to phosphorylate eIF2 $\alpha$ , due to the replacement of the serine residue 71 by an alanine (equivalent to Ser-51 in mammals), are less viable than wild type after incubation in the extracellular milieu, suggesting that phosphorylation of eIF2 $\alpha$  takes place at the time of egress and promotes parasite survival until the next reinvasion (68). *TgSlp* protein shares similar features with mammalian PTP-1B, including its ER localization and possibly its tyrosine phosphatase activity. Therefore, if *Slp* does indeed regulate the ER stress via *TgIF2K-A/eIF2 $\alpha$*  when the tachyzoites become extracellular, the much more stressful environment encountered by the parasite *in vivo* compared to *in vitro* might account for the difference of phenotype observed between the two growth conditions. Whether *Slp* participates in the regulation of the UPR remains to be explored.

Overall, our data identified *Shelph* as an important phosphatase for *Toxoplasma* virulence. As this family of bacterial-like phosphatases are absent from human genomes, it will be relevant to explore their functions in other stages of the parasite life cycle, as they may represent future candidates for therapeutic interventions.

## MATERIALS AND METHODS

**Parasite strains, cell culture, and transfection.** All *T. gondii* parasite strains were generated from *T. gondii* RH- $\Delta ku80$  strain (69), abbreviated  $\Delta ku80$  throughout the study. Parasites were maintained and passaged *in vitro* on human foreskin fibroblasts (HFFs; ATCC CRL 1634) in Dulbecco's modified Eagle's medium (Gibco BRL) supplemented with 5% fetal calf serum (FCS), 2 mM glutamine, and penicillin-streptomycin (Gibco) at 100  $\mu$ g/mL, 37°C, 5% CO<sub>2</sub>. Freshly egressed parasites were transfected by electroporation as described previously (70). Transgenic parasites were selected with 2  $\mu$ M pyrimethamine for pYFP-LIC-DHFR integration, 25  $\mu$ g/mL mycophenolic acid and 50  $\mu$ g/mL xanthine for *HXGPRT* cassette selection, 5  $\mu$ M fluorodeoxyuridine for pUPRT-MIC2-Gluc, and 30  $\mu$ g/mL phleomycin for PSBLE35 cosmid. All the transgenic lines obtained were verified by diagnostic PCR and sequencing.

**Molecular biology.** For cloning, PCRs were performed using Q5 high-fidelity DNA polymerase (New England Biolabs), and all the fragments were sequenced before further use. PCRs amplicons directly used for parasite transfections were amplified with KOD polymerase (Novagen). Integrative PCRs were done using the GoTaq master mix (Promega). RNA extraction and reverse transcription (RT) were performed using the NucleoSpin RNA kit (Macherey-Nagel) and the Superscript first-strand synthesis system (Invitrogen), respectively, according to the manufacturers' instructions. *zfp2* and *slp* cDNAs were amplified using primers ML2877/ML2878 and ML1279/ML1280, respectively. All the primers used in this study are listed in Table S1 in the supplemental material.

**Plasmids. (i) SIp-HA<sub>3</sub>Ct.** SIp-HA<sub>3</sub>Ct parasites were obtained by fusing a triple HA tag (HA<sub>3</sub>) at the 3' end of the *slp* gene using the pYFP-LIC-DHFR vector (69). Briefly, a fragment of 1,260 bp of *slp* was amplified using primers ML1279 and ML1280, containing complementary LIC sequences, and inserted by ligation-independent cloning in pYFP-LIC-DHFR. The resulting plasmid was linearized with EcoRV before transfection of RH $\Delta ku80$  parasites. Single homologous recombination allowed the integration of the whole plasmid, generating the SIp-HA<sub>3</sub>Ct line.

**(ii) SIp-HA<sub>3</sub>.** Three overlapping PCR fragments corresponding to *Shelph* amino acids 335 to 407, HA<sub>3</sub> tag, and *Shelph* amino acids 408 to 421 with 194 bp of the 3'-UTR were amplified using primers MLa140/MLa141, MLa142/MLa171, and MLa144/MLa145, respectively. A long PCR fragment of 540 bp was then obtained with the KOD DNA polymerase by mixing the 3 PCR products and primers MLa140 and MLa145. In addition, a guide RNA targeting amino acids 396 to 402 (gRNA MLa95bis-96 bis) was cloned into the Bsal restriction site of the pU6-Universal plasmid (71).

**(iii) SIp-KO and complementation.** To knock out the *slp* locus in the SIp-HA<sub>3</sub>Ct background, we used CRISPR-Cas9 technology. The guide RNA was obtained by annealing of primers MLa97 and MLa98, followed by Bsal cloning in the pU6-Universal vector. The donor DNA consisted of the PCR amplification of the *HXGPRT* cassette flanked on both sides by 30-bp of homology to the *slp* locus with primers MLa93 and MLa100. Thirty micrograms of pU6-gRNA was cotransfected with 50  $\mu$ L of PCR product in the SIp-HA<sub>3</sub>Ct line. Transgenic parasites were selected with mycophenolic acid and xanthine.

Complementation of SIp-KO parasites was obtained by transfection of PSBLE95 cosmid, followed by selection with phleomycin and cloning by limiting dilution.

**(iv) pUPRT-MIC2-Gluc.** A 4.7-kb fragment comprising the MIC2 promoter, the *mic2* gene fused to *Gaussia* luciferase, and the *mic2* 3'-UTR was amplified using primers ML4941 and ML4942 from pMIC2-GLuc-cMyc (6) and cloned by in-fusion HD (TaKaRa) in the pUPRT-TUB-TgRASP2-Ty plasmid (72), opened with NotI/AvrII restriction sites. The resulting pUPRT-MIC2-Gluc vector was linearized with NdeI prior to transfection and then cotransfected along with pU6-UPRT plasmid encoding a guide RNA targeting the *uprt* locus (70).

**(v) pGex4T3-SIp.** *Slp* protein was expressed as an N-terminal GST-fusion protein. The sequence corresponding to amino acids 84 to 450 of SIp-HA<sub>3</sub> was amplified by PCR from the genomic DNA of SIp-HA<sub>3</sub> parasites using primers MLa383 and MLa384 and then cloned in-frame with GST into XhoI and EcoRI restriction sites of the pGex4T3 vector (GE Healthcare Life Sciences). The resulting vector was transformed into the BL21-DE3(pLysS) bacterial strain (Novagen).

**Recombinant protein purification and phosphatase assay.** *E. coli* cells expressing either the control recombinant GST (rGST) protein or GST-SIp-HA<sub>3</sub> (rSlp) were induced during exponential growth with

0.5 mM isopropyl- $\beta$ -D-thiogalactopyranoside at 37°C for 3 h, and the bacterial cell pellets were lysed using a French press. The soluble recombinants recovered from the supernatants were affinity purified on glutathione-agarose beads (Sigma). Following washes with PBS–0.1% Triton, proteins were eluted in 20 mM reduced glutathione and dialyzed in 20 mM Tris-HCl (pH 8.0), 400 mM NaCl, 0.5 mM MnCl<sub>2</sub> overnight at 4°C.

Phosphatase assays were performed in 100  $\mu$ L reaction buffer (20 mM Tris-HCl [pH 8.0], 400 mM NaCl, 0.5 mM MnCl<sub>2</sub>, 1 mM dithiothreitol) at 37°C for 30 min, with 5 mM pNPP (Bio Basic Inc.) and 0.5  $\mu$ g of protein unless otherwise stated. The absorbance of pNP was read at 405 nm using a Tecan spectrophotometer. To calculate the quantities of pNP released from the reaction, a molar extinction coefficient of 18,000 M<sup>-1</sup> cm<sup>-1</sup> was used.

**Western blotting.** Freshly egressed parasites ( $5 \times 10^6$ ) were lysed in Laemmli buffer and boiled for 5 min. Proteins were separated on an 8 to 12% acrylamide-bisacrylamide gel by SDS-PAGE and transferred onto nitrocellulose membrane. Following blocking in PBS–5% milk for 30 min, the membrane was probed with primary antibodies diluted in PBS–5% milk for 2 h and revealed with secondary antibodies conjugated to alkaline phosphatase (Promega) for 1 h. Proteins were visualized by the addition of color development substrates (nitroblue tetrazolium–5-bromo–4-chloro–3-indolylphosphate; Promega). The antibody dilutions were as follows: rat anti-HA, 1/1,000; mouse anti-SAG1, 1/2,000.

**Immunofluorescence assay.** Following fixation in 4% paraformaldehyde (PAF) for 30 min, cells were permeabilized using PBS–0.1% Triton or PBS-saponin (invasion) for 10 min, then saturated for 30 min in PBS–10% FCS. Primary antibodies diluted in PBS–2% FCS were incubated for 1 h. Following 3 washes in PBS, Alexa-coupled secondary antibodies diluted in PBS–2% FCS were incubated for 1 h. Nuclei were stained with Hoechst for 5 min. Cells were washed 3 times in PBS before mounting. Samples were observed on a Zeiss Axio Imager microscope at the Montpellier RIO Imaging Facility and processed using ZEN software. The antibody dilutions were as follows: rabbit anti-GAP45, 1/5,000 (73); rat anti-HA 3F10, 1/100 (Roche catalog number 11867423001); rabbit anti-AMA1, 1/5,000 (74); mouse anti-MIC3, 1/300 (75); mouse anti-ROP2-4, 1/100 (76); mouse anti-GRA1, 1/300 (77); rabbit anti-GRA2, 1/500 (78); rabbit anti-GRA3, 1/500 (79); mouse anti-SAG1, 1/2,000 (80).

**Invasion, replication, and egress assays.** Freshly egressed parasites ( $5 \times 10^6$  for invasion,  $5 \times 10^5$  for replication and egress) were inoculated on HFFs grown on coverslips for 5 min (invasion) or 1 h (replication, egress) before extensive washes in Hank's balanced salt solution (Gibco BRL). Invasion was stopped by fixation in PAF and further processed for dual-labeling IFA using anti-SAG1 and anti-ROP1 antibodies. Parasite multiplication was allowed to take place for another 24 h (replication) before fixation in PAF and further processing by IFA using anti-SAG1 antibodies. For egress, parasites at 30 h postinvasion were treated with dimethyl sulfoxide (control) or 3  $\mu$ M A23187 for 8 min at 37°C, prior to fixation in PAF and dual labeling using anti-GRA3 and anti-GAP45 antibodies.

**Gliding motility assay.** Freshly egressed parasites ( $1 \times 10^6$ ) were resuspended in 300  $\mu$ L of gliding buffer (155 mM NaCl, 3 mM KCl, 2 mM CaCl<sub>2</sub>, 1 mM MgCl<sub>2</sub>, 3 mM NaH<sub>2</sub>PO<sub>4</sub>, 10 mM HEPES, 10 mM glucose). A 100- $\mu$ L aliquot of this suspension was deposited on a poly-L-lysine-coated slide in a well delineated with a hydrophobic pen. Parasites were allowed to glide for 15 min at 37°C, before fixation in 4% PAF. The slides were further processed by IFA, except that the permeabilization step was omitted. Trails were stained with an anti-SAG1 antibody. Images were processed with ImageJ using the NeuronJ plug-in.

**Microneme secretion assay.** The microneme secretion assay was performed as previously described (6). Briefly, confluent HFF monolayers were inoculated with  $\Delta ku80$ /MIC2Gluc or Slp-KO/MIC2Gluc tachyzoites for 48 h to attain large vacuoles with minimal cell lysis. Infected HFFs were then scraped, shifted to an 18°C water bath to prevent premature microneme secretion, and passed through a 25-gauge needle to release intracellular parasites. After centrifugation ( $400 \times g$ ) for 10 min at 18°C, the parasites were resuspended in EC buffer (5 mM KCl, 142 mM NaCl, 1 mM MgCl<sub>2</sub>, 1.8 mM CaCl<sub>2</sub>, 5.6 mM D-glucose, 25 mM HEPES; pH 7.4). To stimulate microneme secretion, 50  $\mu$ L of mock or 50  $\mu$ L of 1 mM propranolol was added to 50  $\mu$ L EC buffer containing  $5 \times 10^5$  parasites in a 96-well V-bottom plate and incubated in a water bath at 37°C for 10 min. The stimulation was stopped by shifting the plate to ice for 5 min. The supernatant was collected following centrifugation ( $1,200 \times g$ ) for 10 min at 4°C and used to measure the released MIC2-Gluc. The BioLux Gaussia Flex luciferase kit (Pierce) was used according to the manufacturer's instructions. The relative luminescence (RLU) was read on a Centro LB960 luminometer (Berthold Technologies).

**Transmission electron microscopy.** HFF monolayers were infected with  $\Delta ku80$  or Slp-KO parasites and grown for an extra 24 h. They were fixed with 2.5% glutaraldehyde in cacodylate buffer, 0.1 M, pH 7.4. Coverslips were then processed using a Pelco Biowave pro+ (Ted Pella). Briefly, samples were postfixed in 1% OsO<sub>4</sub> and 2% uranyl acetate, dehydrated in an acetone series, and embedded in Epon 118 using the following parameters: glutaraldehyde (150 W on/off/on 1-min cycles); two buffer washes (40 s, 150 W); OsO<sub>4</sub> (150 W on/off/on/off/on 1-min cycles); two water washes (40 s, 150 W); uranyl acetate (100 W on/off/on 1-min cycles); dehydration (40 s, 150 W); and resin infiltration (350 W, 3-min cycles). Fixation and infiltration steps were performed under vacuum. Polymerization was performed at 60°C for 48 h. Ultrathin sections at 70 nM were cut with a Leica UC7 ultramicrotome, counterstained with uranyl acetate and lead citrate, and observed in a Jeol 1400+ transmission electron microscope from the MEA Montpellier Electron Microscopy Platform. All chemicals were from Electron Microscopy Sciences, and solvents were from Sigma.

**Ethics statement.** All mice protocols were approved by the Institutional Animal Care and Utilization Committee (IACUC) of the American University of Beirut (AUB) (permit number 18-02-461). All animals were housed in a specific-pathogen-free facility with a 12-h on/off light cycle. Humane endpoints were fully respected as per AUB IACUC, following Association for Assessment and Accreditation of Laboratory Animal Care International guidelines and the NRC Guide of animal care use book (Guide, NRC 2011). Mice were monitored on a daily basis. To verify the acute phase of the infection, blood was withdrawn following deep anesthesia with isoflurane by inhalation. Mice were sacrificed if any abnormal ethical features were noticed. Animals were deeply anesthetized before cervical dislocation.

**Mouse infection.** Eight- to 10-week-old immunocompetent female BALB/c mice were intraperitoneally injected with  $\Delta ku80$ , Slp-KO, Compl, Slp-HA<sub>3</sub>Ct, or Slp-HA<sub>3</sub> lines. To assess the virulence *in vivo*, freshly harvested tachyzoites ( $10^2$ ,  $10^3$ , or  $>10^4$ ) were intraperitoneally injected into mice. The number of mice used per condition and the number of independent experiments are stated in the legend of each graph. Invasiveness of the parasites was evaluated by simultaneous plaque assay of a similar dose of parasites on HFFs. Immunoreactivity against tachyzoite antigens with serum IgG from mammals having acute toxoplasmosis was used as an indicator of infection (81). For this, on day 6 postinfection, blood samples from each infected mouse were withdrawn using retroorbital puncture. Acute toxoplasmosis was verified by immune reactivity of infected mice with tachyzoite extracts by Western blotting. The seronegative mice were excluded from the analyses. Following mouse injections, their survival was daily monitored until their death, the endpoint of all experiments.

## SUPPLEMENTAL MATERIAL

Supplemental material is available online only.

**FIG S1**, TIF file, 0.5 MB.

**FIG S2**, TIF file, 0.7 MB.

**FIG S3**, TIF file, 0.2 MB.

**FIG S4**, TIF file, 0.3 MB.

**FIG S5**, TIF file, 0.2 MB.

**FIG S6**, TIF file, 1.9 MB.

**FIG S7**, TIF file, 0.9 MB.

**TABLE S1**, DOCX file, 0.02 MB.

## ACKNOWLEDGMENTS

We thank S. Lourido for the pU6-universal and pMIC2-GLuc-cMyc plasmids, Vern Carruthers for the pYFF-LIC-DHFR plasmid, and David Sibley for the PSBLE35 cosmid.

We thank J. F. Dubremetz, M. F. Cesbron-Delauw, and D. Soldati-Favre for antibodies. We thank C. Duperray of the MRI-Cytometry at the Institute for Regenerative Medicine and Biotherapy and the staff of the MRI platform of the University of Montpellier for assistance and technical support.

This work was supported by the Laboratoire d'Excellence Parafrap (ANR-11-LABX-0024) and by the ANR (ANR-21-CE15-0043).

## REFERENCES

- Dubey JP. 2020. The history and life cycle of *Toxoplasma gondii*, p 1–19. In Weiss LM, Kim K (ed), *Toxoplasma gondii*, 3rd ed. Elsevier, Philadelphia, PA.
- Frenkel JK. 1988. Pathophysiology of toxoplasmosis. *Parasitol Today* 4: 273–278. [https://doi.org/10.1016/0169-4758\(88\)90018-x](https://doi.org/10.1016/0169-4758(88)90018-x).
- Gazzinelli RT, Hakim FT, Hieny S, Shearer GM, Sher A. 1991. Synergistic role of CD4<sup>+</sup> and CD8<sup>+</sup> T lymphocytes in IFN-gamma production and protective immunity induced by an attenuated *Toxoplasma gondii* vaccine. *J Immunol* 146: 286–292.
- Yap GS, Sher A. 1999. Effector cells of both nonhemopoietic and hemopoietic origin are required for interferon (IFN)-gamma- and tumor necrosis factor (TNF)-alpha-dependent host resistance to the intracellular pathogen, *Toxoplasma gondii*. *J Exp Med* 189:1083–1092. <https://doi.org/10.1084/jem.189.7.1083>.
- Luft BJ, Remington JS. 1992. Toxoplasmic encephalitis in AIDS. *Clin Infect Dis* 15:211–222. <https://doi.org/10.1093/clinids/15.2.211>.
- Brown KM, Lourido S, Sibley LD. 2016. Serum albumin stimulates protein kinase G-dependent microneme secretion in *Toxoplasma gondii*. *J Biol Chem* 291:9554–9565. <https://doi.org/10.1074/jbc.M115.700518>.
- Brown KM, Long S, Sibley LD. 2017. Plasma membrane association by N-acylation governs PKG function in *Toxoplasma gondii*. *mBio* 8. <https://doi.org/10.1128/mBio.00375-17>.
- Wiersma HJ, Galuska SE, Tomley FM, Sibley LD, Liberator PA, Donald RGK. 2004. A role for coccidian cGMP-dependent protein kinase in motility and invasion. *Int J Parasitol* 34:369–380. <https://doi.org/10.1016/j.ijpara.2003.11.019>.
- Donald RGK, Zhong T, Wiersma H, Nare B, Yao D, Lee A, Allocco J, Liberator PA. 2006. Anticoccidial kinase inhibitors: identification of protein kinase targets secondary to cGMP-dependent protein kinase. *Mol Biochem Parasitol* 149: 86–98. <https://doi.org/10.1016/j.molbiopara.2006.05.003>.
- Howard BL, Harvey KL, Stewart RJ, Azevedo MF, Crabb BS, Jennings IG, Sanders PR, Manallack DT, Thompson PE, Tonkin CJ, Gilson PR. 2015. Identification of potent phosphodiesterase inhibitors that demonstrate cyclic nucleotide-dependent functions in apicomplexan parasites. *ACS Chem Biol* 10: 1145–1154. <https://doi.org/10.1021/cb501004q>.
- Jia Y, Marq J-B, Bisio H, Jacot D, Mueller C, Yu L, Choudhary J, Brochet M, Soldati-Favre D. 2017. Crosstalk between PKA and PKG controls pH-dependent host cell egress of *Toxoplasma gondii*. *EMBO J* 36:3250–3267. <https://doi.org/10.15252/emboj.201796794>.
- Kurokawa H, Kato K, Iwanaga T, Sugi T, Sudo A, Kobayashi K, Gong H, Takemae H, Recuenco FC, Horimoto T, Akashi H. 2011. Identification of *Toxoplasma gondii* cAMP dependent protein kinase and its role in the tachyzoite growth. *PLoS One* 6:e22492. <https://doi.org/10.1371/journal.pone.0022492>.
- Uboldi AD, Wilde M-L, McRae EA, Stewart RJ, Dagley LF, Yang L, Katris NJ, Hapuarachchi SV, Coffey MJ, Lehane AM, Botte CY, Waller RF, Webb AI, McConville MJ, Tonkin CJ. 2018. Protein kinase A negatively regulates Ca<sup>2+</sup> signalling in *Toxoplasma gondii*. *PLoS Biol* 16:e2005642. <https://doi.org/10.1371/journal.pbio.2005642>.
- Kirkman LA, Weiss LM, Kim K. 2001. Cyclic nucleotide signaling in *Toxoplasma gondii* bradyzoite differentiation. *Infect Immun* 69:148–153. <https://doi.org/10.1128/IAI.69.1.148-153.2001>.
- Eaton MS, Weiss LM, Kim K. 2006. Cyclic nucleotide kinases and tachyzoite-bradyzoite transition in *Toxoplasma gondii*. *Int J Parasitol* 36:107–114. <https://doi.org/10.1016/j.ijpara.2005.08.014>.
- Sugi T, Ma YF, Tomita T, Murakoshi F, Eaton MS, Yakubu R, Han B, Tu V, Kato K, Kawazu S-I, Gupta N, Suvorova ES, White MW, Kim K, Weiss LM. 2016. *Toxoplasma gondii* cyclic AMP-dependent protein kinase subunit 3 is involved in the switch from tachyzoite to bradyzoite development. *mBio* 7:e00755-16. <https://doi.org/10.1128/mBio.00755-16>.
- Nagamune K, Sibley LD. 2006. Comparative genomic and phylogenetic analyses of calcium ATPases and calcium-regulated proteins in the Apicomplexa. *Mol Biol Evol* 23:1613–1627. <https://doi.org/10.1093/molbev/msl026>.
- Garrison E, Treeck M, Ehret E, Butz H, Garbuz T, Oswald BP, Settles M, Boothroyd J, Arrizabalaga G. 2012. A forward genetic screen reveals that

- calcium-dependent protein kinase 3 regulates egress in *Toxoplasma*. PLoS Pathog 8:e1003049. <https://doi.org/10.1371/journal.ppat.1003049>.
19. Lourido S, Shuman J, Zhang C, Shokat KM, Hui R, Sibley LD. 2010. Calcium-dependent protein kinase 1 is an essential regulator of exocytosis in *Toxoplasma*. *Nature* 465:359–362. <https://doi.org/10.1038/nature09022>.
  20. Trecek M, Sanders JL, Gaji RY, LaFavers KA, Child MA, Arrizabalaga G, Elias JE, Boothroyd JC. 2014. The calcium-dependent protein kinase 3 of *Toxoplasma* influences basal calcium levels and functions beyond egress as revealed by quantitative phosphoproteome analysis. PLoS Pathog 10:e1004197. <https://doi.org/10.1371/journal.ppat.1004197>.
  21. Moorhead GBG, De Wever V, Templeton G, Kerk D. 2009. Evolution of protein phosphatases in plants and animals. *Biochem J* 417:401–409. <https://doi.org/10.1042/BJ20081986>.
  22. Yang C, Arrizabalaga G. 2017. The serine/threonine phosphatases of apicomplexan parasites: serine/threonine phosphatases of apicomplexa. *Mol Microbiol* 106:1–21. <https://doi.org/10.1111/mmi.13715>.
  23. Andreeva AV, Kutuzov MA. 2004. Widespread presence of “bacterial-like” PPP phosphatases in eukaryotes. *BMC Evol Biol* 4:47. <https://doi.org/10.1186/1471-2148-4-47>.
  24. Uhrig RG, Moorhead GB. 2011. Two ancient bacterial-like PPP family phosphatases from *Arabidopsis* are highly conserved plant proteins that possess unique properties. *Plant Physiol* 157:1778–1792. <https://doi.org/10.1104/pp.111.182493>.
  25. Uhrig RG, Labandera A-M, Tang L-Y, Sieben NA, Goudreault M, Yeung E, Gingras A-C, Samuel MA, Moorhead GBG. 2017. Activation of mitochondrial protein phosphatase SLP2 by MIA40 regulates seed germination. *Plant Physiol* 173:956–969. <https://doi.org/10.1104/pp.16.01641>.
  26. Fernandez-Pol S, Slouka Z, Bhattacharjee S, Fedotova Y, Freed S, An X, Holder AA, Campanella E, Low PS, Mohandas N, Haldar K. 2013. A bacterial phosphatase-like enzyme of the malaria parasite *Plasmodium falciparum* possesses tyrosine phosphatase activity and is implicated in the regulation of band 3 dynamics during parasite invasion. *Eukaryot Cell* 12:1179–1191. <https://doi.org/10.1128/EC.00027-13>.
  27. Patzewitz E-M, Guttery D, Poulin B, Ramakrishnan C, Ferguson DP, Wall R, Brady D, Holder A, Szöör B, Tewari R. 2013. An ancient protein phosphatase, SHLP1, is critical to microneme development in *Plasmodium* ookinetes and parasite transmission. *Cell Rep* 3:622–629. <https://doi.org/10.1016/j.celrep.2013.01.032>.
  28. Miliu A, Lebrun M, Braun-Breton C, Lamarque MH. 2017. Shelph2, a bacterial-like phosphatase of the malaria parasite *Plasmodium falciparum*, is dispensable during asexual blood stage. PLoS One 12:e0187073. <https://doi.org/10.1371/journal.pone.0187073>.
  29. Liang Q-L, Nie L-B, Li T-T, Elsheikha HM, Sun L-X, Zhang Z-W, Zhao D-Y, Zhu X-Q, Wang J-L. 2021. Functional characterization of 17 protein serine/threonine phosphatases in *Toxoplasma gondii* using CRISPR-Cas9 system. *Front Cell Dev Biol* 9:738794. <https://doi.org/10.3389/fcell.2021.738794>.
  30. Lewis MJ, Pelham HRB. 1990. A human homologue of the yeast HDEL receptor. *Nature* 348:162–163. <https://doi.org/10.1038/348162a0>.
  31. Semenza JC, Hardwick KG, Dean N, Pelham HRB. 1990. ERD2, a yeast gene required for the receptor-mediated retrieval of luminal ER proteins from the secretory pathway. *Cell* 61:1349–1357. [https://doi.org/10.1016/0092-8674\(90\)90698-E](https://doi.org/10.1016/0092-8674(90)90698-E).
  32. Behnke MS, Wootton JC, Lehmann MM, Radke JB, Lucas O, Nawas J, Sibley LD, White MW. 2010. Coordinated progression through two subtranscriptomes underlies the tachyzoite cycle of *Toxoplasma gondii*. PLoS One 5:e12354. <https://doi.org/10.1371/journal.pone.0012354>.
  33. Barylyuk K, Koreny L, Ke H, Butterworth S, Crook OM, Lassadi I, Gupta V, Tromer E, Mourier T, Stevens TJ, Breckels LM, Pain A, Lilley KS, Waller RF. 2020. A comprehensive subcellular atlas of the *Toxoplasma* proteome via hyperLOPIT provides spatial context for protein functions. *Cell Host Microbe* 28:752–766.e9. <https://doi.org/10.1016/j.chom.2020.09.011>.
  34. Tsuruta H, Aizono Y. 2003. Catalytic efficiency and some structural properties of cold-active protein-tyrosine-phosphatase. *J Biochem* 133:225–230. <https://doi.org/10.1093/jb/mvg029>.
  35. Sidik SM, Huet D, Ganesan SM, Huynh M-H, Wang T, Nasamu AS, Thiru P, Saeji J, Carruthers VB, Niles JC, Lourido S. 2016. A genome-wide CRISPR screen in *Toxoplasma* identifies essential apicomplexan genes. *Cell* 166:1423–1435.e12. <https://doi.org/10.1016/j.cell.2016.08.019>.
  36. Gubbels M-J, Lehmann M, Muthalagi M, Jerome ME, Brooks CF, Szatanek T, Flynn J, Parrot B, Radke J, Striepen B, White MW. 2008. Forward genetic analysis of the apicomplexan cell division cycle in *Toxoplasma gondii*. PLoS Pathog 4:e36. <https://doi.org/10.1371/journal.ppat.0040036>.
  37. Kremer K, Kamin D, Rittweger E, Wilkes J, Flammer H, Mahler S, Heng J, Tonkin CJ, Langsley G, Hell SW, Carruthers VB, Ferguson DJP, Meissner M. 2013. An overexpression screen of *Toxoplasma gondii* Rab-GTPases reveals distinct transport routes to the micronemes. PLoS Pathog 9:e1003213. <https://doi.org/10.1371/journal.ppat.1003213>.
  38. Bullen HE, Jia Y, Yamaro-Botté Y, Bisio H, Zhang O, Jemelin NK, Marq J-B, Carruthers V, Botté CY, Soldati-Favre D. 2016. Phosphatidic acid-mediated signaling regulates microneme secretion in *Toxoplasma*. *Cell Host Microbe* 19:349–360. <https://doi.org/10.1016/j.chom.2016.02.006>.
  39. Sangaré LO, Ólafsson EB, Wang Y, Yang N, Julien L, Camejo A, Pesavento P, Sidik SM, Lourido S, Barragan A, Saeji J. 2019. In vivo CRISPR screen identifies TgWIP as a *Toxoplasma* modulator of dendritic cell migration. *Cell Host Microbe* 26:478–492.e8. <https://doi.org/10.1016/j.chom.2019.09.008>.
  40. Wang Y, Sangaré LO, Paredes-Santos TC, Hassan MA, Krishnamurthy S, Furuta AM, Markus BM, Lourido S, Saeji J. 2020. Genome-wide screens identify *Toxoplasma gondii* determinants of parasite fitness in IFN- $\gamma$ -activated murine macrophages. *Nat Commun* 11:5258. <https://doi.org/10.1038/s41467-020-18991-8>.
  41. Young J, Dominicus C, Wagener J, Butterworth S, Ye X, Kelly G, Ordan M, Saunders B, Instrell R, Howell M, Stewart A, Trecek M. 2019. A CRISPR platform for targeted in vivo screens identifies *Toxoplasma gondii* virulence factors in mice. *Nat Commun* 10:3963. <https://doi.org/10.1038/s41467-019-11855-w>.
  42. Hakimi M-A, Olias P, Sibley LD. 2017. *Toxoplasma* effectors targeting host signaling and transcription. *Clin Microbiol Rev* 30:615–645. <https://doi.org/10.1128/CMR.00005-17>.
  43. Krishnan A, Kloehn J, Lunghi M, Chiappino-Pepe A, Waldman BS, Nicolas D, Varesio E, Hehl A, Lourido S, Hatzimanikatis V, Soldati-Favre D. 2020. Functional and computational genomics reveal unprecedented flexibility in stage-specific *Toxoplasma* metabolism. *Cell Host Microbe* 27:290–306.e11. <https://doi.org/10.1016/j.chom.2020.01.002>.
  44. Fox BA, Bzik DJ. 2002. De novo pyrimidine biosynthesis is required for virulence of *Toxoplasma gondii*. *Nature* 415:926–929. <https://doi.org/10.1038/415926a>.
  45. Munro S, Pelham HR. 1987. A C-terminal signal prevents secretion of luminal ER proteins. *Cell* 48(5):899–907. [https://doi.org/10.1016/0092-8674\(87\)90086-9](https://doi.org/10.1016/0092-8674(87)90086-9).
  46. Scott M, Lu G, Hallett M, Thomas DY. 2004. The Hera database and its use in the characterization of endoplasmic reticulum proteins. *Bioinformatics* 20:937–944. <https://doi.org/10.1093/bioinformatics/bth010>.
  47. Venugopal K, Marion S. 2018. Secretory organelle trafficking in *Toxoplasma gondii*: a long story for a short travel. *Int J Med Microbiol* 308:751–760. <https://doi.org/10.1016/j.ijmm.2018.07.007>.
  48. Sangaré LO, Alayi TD, Westermann B, Hovasse A, Sindikubwabo F, Callebaut I, Werkmeister E, Lafont F, Slomianny C, Hakimi M-A, Van Dorselaer A, Schaeffer-Reiss C, Tomavo S. 2016. Unconventional endosome-like compartment and retromer complex in *Toxoplasma gondii* govern parasite integrity and host infection. *Nat Commun* 7:11191. <https://doi.org/10.1038/ncomms11191>.
  49. Ngô HM, Yang M, Paprotka K, Pypaert M, Hoppe H, Joiner KA. 2003. AP-1 in *Toxoplasma gondii* mediates biogenesis of the rhoptry secretory organelle from a post-Golgi compartment. *J Biol Chem* 278:5343–5352. <https://doi.org/10.1074/jbc.M208291200>.
  50. Hoppe HC, Ngô HM, Yang M, Joiner KA. 2000. Targeting to rhoptry organelles of *Toxoplasma gondii* involves evolutionarily conserved mechanisms. *Nat Cell Biol* 2:449–456. <https://doi.org/10.1038/35017090>.
  51. Di Cristina M, Spaccapelo R, Soldati D, Bistoni F, Crisanti A. 2000. Two conserved amino acid motifs mediate protein targeting to the micronemes of the apicomplexan parasite *Toxoplasma gondii*. *Mol Cell Biol* 20:7332–7341. <https://doi.org/10.1128/MCB.20.19.7332-7341.2000>.
  52. Dubey JP, Lindsay DS, Speer CA. 1998. Structures of *Toxoplasma gondii* tachyzoites, bradyzoites, and sporozoites and biology and development of tissue cysts. *Clin Microbiol Rev* 11:267–299. <https://doi.org/10.1128/CMR.11.2.267>.
  53. Ramakrishnan C, Maier S, Walker RA, Rehrauer H, Joekel DE, Winiger RR, Basso WU, Grigg ME, Hehl AB, Deplazes P, Smith NC. 2019. An experimental genetically attenuated live vaccine to prevent transmission of *Toxoplasma gondii* by cats. *Sci Rep* 9:1474. <https://doi.org/10.1038/s41598-018-37671-8>.
  54. Hehl AB, Basso WU, Lippuner C, Ramakrishnan C, Okoniewski M, Walker RA, Grigg ME, Smith NC, Deplazes P. 2015. Asexual expansion of *Toxoplasma gondii* merozoites is distinct from tachyzoites and entails expression of non-overlapping gene families to attach, invade, and replicate within feline enterocytes. *BMC Genomics* 16:66. <https://doi.org/10.1186/s12864-015-1225-x>.
  55. Garfoot AL, Wilson GM, Coon JJ, Knoll LJ. 2019. Proteomic and transcriptomic analyses of early and late-chronic *Toxoplasma gondii* infection shows novel and stage specific transcripts. *BMC Genomics* 20:859. <https://doi.org/10.1186/s12864-019-6213-0>.
  56. Read A, Schröder M. 2021. The unfolded protein response: an overview. *Biology* 10:384. <https://doi.org/10.3390/biology10050384>.

57. Sullivan WJ, Narasimhan J, Bhatti MM, Wek RC. 2004. Parasite-specific eIF2 (eukaryotic initiation factor-2) kinase required for stress-induced translation control. *Biochem J* 380:523–531. <https://doi.org/10.1042/BJ20040262>.
58. Narasimhan J, Joyce BR, Naguleswaran A, Smith AT, Livingston MR, Dixon SE, Coppens I, Wek RC, Sullivan WJ. 2008. Translation regulation by eukaryotic initiation factor-2 kinases in the development of latent cysts in *Toxoplasma gondii*. *J Biol Chem* 283:16591–16601. <https://doi.org/10.1074/jbc.M800681200>.
59. Harding HP, Zhang Y, Ron D. 1999. Protein translation and folding are coupled by an endoplasmic-reticulum-resident kinase. *Nature* 397:271–274. <https://doi.org/10.1038/16729>.
60. Sood R, Porter AC, Ma K, Quilliam LA, Wek RC. 2000. Pancreatic eukaryotic initiation factor-2alpha kinase (PEK) homologues in humans, *Drosophila melanogaster* and *Caenorhabditis elegans* that mediate translational control in response to endoplasmic reticulum stress. *Biochem J* 346:281–293. <https://doi.org/10.1042/bj3460281>.
61. Su Q, Wang S, Gao HQ, Kazemi S, Harding HP, Ron D, Koromilas AE. 2008. Modulation of the eukaryotic initiation factor 2 alpha-subunit kinase PERK by tyrosine phosphorylation. *J Biol Chem* 283:469–475. <https://doi.org/10.1074/jbc.M704612200>.
62. Marciniak SJ, Garcia-Bonilla L, Hu J, Harding HP, Ron D. 2006. Activation-dependent substrate recruitment by the eukaryotic translation initiation factor 2 kinase PERK. *J Cell Biol* 172:201–209. <https://doi.org/10.1083/jcb.200508099>.
63. Krishnan N, Fu C, Pappin DJ, Tonks NK. 2011. H2S-induced sulfhydrylation of the phosphatase PTP1B and its role in the endoplasmic reticulum stress response. *Sci Signal* 4:ra86. <https://doi.org/10.1126/scisignal.2002329>.
64. Bakke J, Haj FG. 2015. Protein-tyrosine phosphatase 1B substrates and metabolic regulation. *Semin Cell Dev Biol* 37:58–65. <https://doi.org/10.1016/j.semcdb.2014.09.020>.
65. Feldhammer M, Uetani N, Miranda-Saavedra D, Tremblay ML. 2013. PTP1B: a simple enzyme for a complex world. *Crit Rev Biochem Mol Biol* 48:430–445. <https://doi.org/10.3109/10409238.2013.819830>.
66. Bettaieb A, Matsuo K, Matsuo I, Wang S, Melhem R, Koromilas AE, Haj FG. 2012. Protein tyrosine phosphatase 1B deficiency potentiates PERK/eIF2 $\alpha$  signaling in brown adipocytes. *PLoS One* 7:e34412. <https://doi.org/10.1371/journal.pone.0034412>.
67. Bettaieb A, Liu S, Xi Y, Nagata N, Matsuo K, Matsuo I, Chahed S, Bakke J, Keilhack H, Tiganis T, Haj FG. 2011. Differential regulation of endoplasmic reticulum stress by protein tyrosine phosphatase 1B and T cell protein tyrosine phosphatase. *J Biol Chem* 286:9225–9235. <https://doi.org/10.1074/jbc.M110.186148>.
68. Joyce BR, Queener SF, Wek RC, Sullivan WJ. 2010. Phosphorylation of eukaryotic initiation factor-2{alpha} promotes the extracellular survival of obligate intracellular parasite *Toxoplasma gondii*. *Proc Natl Acad Sci U S A* 107:17200–17205. <https://doi.org/10.1073/pnas.1007610107>.
69. Huynh M-H, Carruthers VB. 2009. Tagging of endogenous genes in a *Toxoplasma gondii* strain lacking Ku80. *Eukaryot Cell* 8:530–539. <https://doi.org/10.1128/EC.00358-08>.
70. Guérin A, Corrales RM, Parker ML, Lamarque MH, Jacot D, El Hajj H, Soldati-Favre D, Boulanger MJ, Lebrun M. 2017. Efficient invasion by *Toxoplasma* depends on the subversion of host protein networks. *Nat Microbiol* 2:1358–1366. <https://doi.org/10.1038/s41564-017-0018-1>.
71. Sidik SM, Hackett CG, Tran F, Westwood NJ, Lourido S. 2014. Efficient genome engineering of *Toxoplasma gondii* using CRISPR/Cas9. *PLoS One* 9:e100450. <https://doi.org/10.1371/journal.pone.0100450>.
72. Suarez C, Lentini G, Ramaswamy R, Maynadier M, Aquilini E, Berry-Sterkers L, Cipriano M, Chen AL, Bradley P, Striepen B, Boulanger MJ, Lebrun M. 2019. A lipid-binding protein mediates rhoptry discharge and invasion in *Plasmodium falciparum* and *Toxoplasma gondii* parasites. *Nat Commun* 10:4041. <https://doi.org/10.1038/s41467-019-11979-z>.
73. Plattner F, Yarovinsky F, Romero S, Didry D, Carlier M-F, Sher A, Soldati-Favre D. 2008. *Toxoplasma* profilin is essential for host cell invasion and TLR11-dependent induction of an interleukin-12 response. *Cell Host Microbe* 3:77–87. <https://doi.org/10.1016/j.chom.2008.01.001>.
74. Lamarque M, Besteiro S, Papoin J, Roques M, Vulliez-Le Normand B, Morlon-Guyot J, Dubremetz J-F, Fauquenoy S, Tomavo S, Faber BW, Kocken CH, Thomas AW, Boulanger MJ, Bentley GA, Lebrun M. 2011. The RON2-AMA1 interaction is a critical step in moving junction-dependent invasion by apicomplexan parasites. *PLoS Pathog* 7:e1001276. <https://doi.org/10.1371/journal.ppat.1001276>.
75. Achbarou A, Mercereau-Puijalon O, Autheman JM, Fortier B, Camus D, Dubremetz JF. 1991. Characterization of microneme proteins of *Toxoplasma gondii*. *Mol Biochem Parasitol* 47:223–233. [https://doi.org/10.1016/0166-6851\(91\)90182-6](https://doi.org/10.1016/0166-6851(91)90182-6).
76. Héron P, Hernández-Pando R, Dubremetz JF, Saavedra R. 1993. Subcellular localization of the 54-kDa antigen of *Toxoplasma gondii*. *J Parasitol* 79:216–222. <https://doi.org/10.2307/3283510>.
77. Charif H, Darcy F, Torpier G, Cesbron-Delauw M-F, Capron A. 1990. *Toxoplasma gondii*: characterization and localization of antigens secreted from tachyzoites. *Exp Parasitol* 71:114–124. [https://doi.org/10.1016/0014-4894\(90\)90014-4](https://doi.org/10.1016/0014-4894(90)90014-4).
78. Labruyere E, Lingnau M, Mercier C, Sibley LD. 1999. Differential membrane targeting of the secretory proteins GRA4 and GRA6 within the parasitophorous vacuole formed by *Toxoplasma gondii*. *Mol Biochem Parasitol* 102:311–324. [https://doi.org/10.1016/s0166-6851\(99\)00092-4](https://doi.org/10.1016/s0166-6851(99)00092-4).
79. Achbarou A, Mercereau-Puijalon O, Sadak A, Fortier B, Leriche MA, Camus D, Dubremetz JF. 1991. Differential targeting of dense granule proteins in the parasitophorous vacuole of *Toxoplasma gondii*. *Parasitology* 103:321–329. <https://doi.org/10.1017/S0031182000059837>.
80. Couvreur G, Sadak A, Fortier B, Dubremetz JF. 1988. Surface antigens of *Toxoplasma gondii*. *Parasitology* 97:1–10. <https://doi.org/10.1017/S0031182000066695>.
81. Erlich HA, Rodgers G, Vaillancourt P, Araujo FG, Remington JS. 1983. Identification of an antigen-specific immunoglobulin M antibody associated with acute *Toxoplasma* infection. *Infect Immun* 41:683–690. <https://doi.org/10.1128/iai.41.2.683-690.1983>.